The Opposing Roles of H2A and H2B Ubiquitination on Nucleosome Dynamics Revealed by Molecular Simulations

Lokesh Baweja[†,¶] and Jeff Wereszczynski[*,‡,¶]

†*Department of Physics, Illinois Institute of Technology, Chicago, USA*

‡*Departments of Physics and Biology, Illinois Institute of Technology, Chicago, USA*

¶*Center for Molecular Study of Condensed Soft Matter, Illinois Institute of Technology, Chicago, USA*

E-mail: jwereszc@iit.edu

Abstract

Nucleosome ubiquitination at lysine 119 of histone H2A (H2AK119Ub) and lysine 120 of histone H2B (H2BK120Ub) are prominent post-translational modifications with opposing roles in chromatin regulation. While H2AK119Ub is associated with transcriptional repression, H2BK120Ub promotes activation, yet the structural mechanisms underlying these effects remain poorly understood due to experimental limitations. To address this, we employed microsecond-scale all-atom molecular dynamics and coarse-grained simulations to investigate the impact of ubiquitination at these sites on nucleosome dynamics. Our results reveal that ubiquitin interacts weakly with DNA in both cases but exhibits higher affinity in H2AK119Ub. Notably, H2AK119Ub stabilizes the nucleosome by strengthening tetramer-dimer and dimer-dimer interactions, particularly at the L1-L1 loop regions, through long-range contacts. In contrast, H2BK120Ub disrupts these interactions, destabilizing the nucleosome and promoting transitions

toward hexasomal and tetrasomal states, as observed in coarse-grained nucleosome folding simulations. These findings suggest that ubiquitination directly modulates nucleosome stability and dynamics in a site-dependent manner, providing a mechanistic framework for how chromatin structure is tuned through post-translational modifications.

Introduction

The nucleosome core particle (NCP) is the fundamental unit of chromatin, where approximately 147 base pairs of DNA are tightly wrapped around a histone core, which is formed by the association of an $(H3/H4)_2$ tetramer with two H2A/H2B dimers[1–4]. Each histone is composed of three alpha helices (referred to as α1, α2, and α3) along with disordered histone "tails" of various lengths that protrude from the core[5]. At physiological salt concentrations the histone octamer is only stable in the presence of wrapped DNA or high salt concentration due to the high positive charge of the individual histones[6,7].

The strong association of DNA with the histone core sterically occludes the DNA-binding sites required for vital cellular process such as transcriptional regulation and DNA repair[8–11]. One mechanism by which histone-DNA and histone-histone interactions are modulated to tune DNA accessibly is through histone modifying post-translational modifications (PTMs)[12,13]. Histone modifications differ in type and size; for instance, acetylation, methylation, and phosphorylation are small chemical modifications, while ubiquitination involves the addition of 76 amino acids through an isopeptide bond and introduces both steric bulk and additional residues for DNA interactions within the nucleosome[14–16]. Ubiquitination occurs predominantly in the histones H2A and H2B, accounting for approximately 10-15% of the total histone PTMs[17–19], while less than 0.3% and 0.1% of the histones H3 and H4[20], respectively, are ubiquitinated. Two major histone ubiquitination sites have been identified: lysine 119 on H2A (H2AK119ub) and lysine 120 on H2B (H2BK120ub) in higher organisms[21,22]. H2A119Kub is located on the disordered C-terminal tail of H2A near the dyad axis and the entry and exit DNA, whereas H2BK120 resides on an H2B alpha helix near the acidic patch (Figure 1).

In a recent chromatin immunoprecipitation sequencing study by Tamburri *et al.* it was shown that H2AK119 ubiquitination co-exists with H3K27 trimethylation in transcriptionally inactive heterochromatin regions[23]. H2AK119 has also been shown to be required for the high affinity binding of the RING1 and YY1 binding protein (RYBP) protein of polycomb

repressive complex to nucleosome, which are implicated in heterochromatin formation[24]. H2BK120 ubiquitination, on the other hand, is linked to actively transcribed regions and chromatin decompaction[25]. H2BK120ub has been shown to enhance the binding of histone chaperone FACT (Facilitates Chromatin Transcription) complex by decreasing nucleosomal stability[25]. To probe how ubiquinitation affects NCP structures, Xia *et al.*, used single molecule FRET experiments and demonstrated that H2AK119ub reinforces the mechanical stability of the nucleosome, although only weak interactions of ubiquitin with DNA were reported[26].

Despite these excellent experimental studies, the role of ubiquitination in modulating nucleosome dynamics across different timescales remains unclear[27,28]. Recently, a wealth of all-atom and coarse-grain molecular dynamics (MD) simulations have been performed on canonical and modified nucleosome systems that have helped to uncover the effects of histone modifications and variants on nucleosome dynamics as a mechanism of gene regulation[29–36]. Here, to understand how ubiquitin influences nucleosome structures and dynamics, we conducted microsecond-long all-atom and coarse-grain (CG) MD simulations combined with Markov state modeling (MSM)[37]. This approach allowed us to determine the effects of ubiquitination at the sites H2AK119ub and H2BK120ub on nucleosome stability, dynamics, and folding. Our all-atom simulations revealed opposing effects of ubiquitination on nucleosome stability. H2AK119ub enhances nucleosome stability by reinforcing the H2A-H2B dimer within the histone core, significantly strengthening the L1-L1 interface, as suggested by contact and energetic analyses. In contrast, H2BK120ub destabilizes the dimer within the histone core. Folding simulations using CG models further demonstrate that H2BK120ub causes pronounced destabilization of the nucleosomal state, with both ubiquitinations favoring the formation of hexasomal and tetrasomal intermediates. Overall, our findings highlight the site-dependent functional role of ubiquitination in modulating nucleosome dynamics and thus affecting the physical basis of gene expression.

Materials and Methods

System preparation and simulations setup

Initial structures of the canonical and H2AK119 and H2BK120 ubiquitinated nucleosome core particle (NCPs) were constructed using Chimera based on the 1KX5 NCP structure,[38,39] where the DNA was substituted with a Widom 601 DNA sequence.[40] H2AK119 and H2BK120 systems were generated using Chimera by conjugating the ubiquitin moieties at the sites H2AK119 and H2BK120 with an isopeptide linkage.[39] The parameters for the isopepetide linkage were obtained with antechamber using GAFF with partial charges derived from restrained electrostatic potential fitting at the HF/6-31G* using gaussian level 09[41].

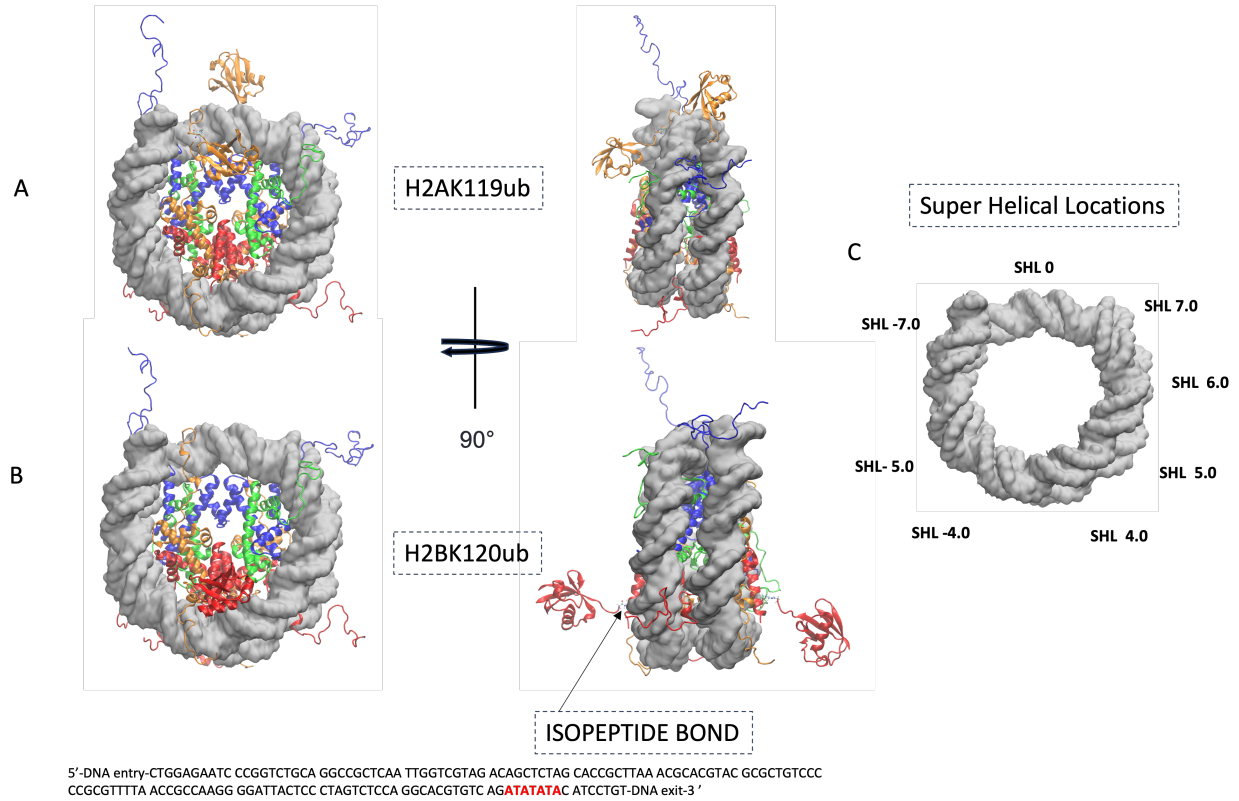

Figure 1: (A-B) Initial conformations of the H2AK119 and H2BK120 ubiquitinated systems generated through Chimera and the Widom 601 nucleotide sequence in 5' to 3' orientation with AT rich DNA exit end. (C) Super helical locations (SHLs) sites marked on nucleosomal DNA.

The protein and DNA in these systems were modeled with the Amber ff19SB[42] and BSC1[43] force fields, respectively. All systems were then solvated with OPC water models[44] with 0.15M KCl. A 4fs timestep was used in conjunction with hydrogen mass repartitioning.[45,46] All systems were first energy minimized for 5000 steps with solute harmonic restraints of 10 kcal/mol/$Å^2$, followed by 5000 steps with no restraints. Minimized systems were then equilibrated for 100 ps by keeping the volume constant and gradually increasing the temperature from 10K to 310K with heavy atom restraints. Afterwards, the heavy atom restraints were gradually decreased over 1000 ps in the isothermal and isobaric ensemble. Production runs were performed in triplicate for 2 µs with Amber 22, accumulation 18 µs of sampling across all three systems (Table S1). Trajectories were recorded every 10 ps and visualized using VMD[47] and PyMol.[48] The last 1.5 µs were analyzed using CPPTRAJ[49] and Python scripts allowing for 500 ns of equilibration.

Coarse grain (CG) simulations used the AICG2+ protein potential[50] and 3SPN2.C DNA sequence-dependent potential models.[51] In these models, each amino acid is treated with a single Cα bead and each nucleotide consists of three beads corresponding to the base, sugar, and phosphate. The flexible histone tails (residues 1-32 for H3, 1-23 for H4, 1-14 and 121-128 for H2A, 1-26 for H2B) were treated with the flexible local potential. The DNA and histones interacted via excluded volume, Debye–Hückel electrostatics and hydrogen bond interactions.[52] The charges for the structured histone core were derived using the RESPAC method,[53] whereas for the flexible tails and ubiquitin moiety we used standard integer charges. Scaling factors of 0.3 and 0.6 were used for non-bonded interactions between the $(H3/H4)_2$ tetramer and H2A/H2B dimers and the DNA/histones, respectively, as used in previous work.[31]

For coarse-graining of ubiquitinated systems, the isopeptide linkage was treated using the flexible local potential present in the cafemol package. The parameter for this linkage were derived from all-atom simulations of K63 linked diubiquitin (PDB ID:3H7S).[54] We coarse-grained the isopeptide bond by placing a Cα bead at the center of mass of the –GLY-

LYS– linkage (Figure S9). We then used a protocol adopted from Terakawa and Takada based on Boltzmann Inversion to obtain (GLY-ISO-LYS) angle and (–GLY-GLY-ISO-LYS–) and (–GLY-ISO-LYS-LYS–) dihedral parameters.[55] We carried out five Boltzmann inversion simulations to capture the bond angle and dihedral distributions obtained from all-atom simulations (Figure S9).

The initial tetrasomal (T), hexasome-left (HL), hexasome-right (HR), and Nucleosome (N) conformations for CG simulation were obtained from our previous study (Figure S1).[56] CG molecular dynamics simulations were conducted using the CafeMol software.[57] Integration of the equations of motion was performed through Langevin dynamics at a temperature of 310 K, employing a timestep of 0.3 CafeMol time units. All units in Coarse-grain simulations are reduced units, where the time step qualitatively corresponds to approximately 30 ps.[31] During CG simulations, harmonic restraints were applied to the $(H3/H4)_2$ tetramer and dyad base pair to ensure the stability of the tetrasomal system. Specifically, the structured region of the two H3 histones experienced restraints with a force constant of 0.001 kcal/mol/Å^2.[31] Additionally, harmonic restraints were imposed on the phosphate beads of the DNA dyad residues with a force constant of 0.1 kcal/mol/Å^2. These restraints limited large-scale sliding of DNA relative to the $(H3/H4)_2$ tetramer while leaving the unbound H2A/H2B dimers unrestricted. This setup is used to mimic the experimental conditions used for nucleosome refolding studies from the tetrasomal states.[58]

Markov State Modeling:

We modelled nucleosome reassembly from tetrasomal states using a set of six collective variables that defined the binding of H2A/H2B dimers with the $(H3\text{-}H4)_2$ interface and the degree of DNA opening. The first two collective variables measured the normalized number of contacts for each dimer with the tetramer. To do this, we measured the distance between the center of mass of the H2B residues 73-100 and the center of mass of the H4 residues 65-92 and normalized it to between 0 and 1. A value close to 1 indicates a dimer bound

to the $(H3/H4)_2$ tetramer in its native configuration and a value close to 0 indicates no dimer/tetramer interactions. The third and fourth collective variables represent the radius of gyration of the entry and exit halves of the DNA. The entry half includes base pairs from the DNA end up to the dyad, while the exit half consists of the remaining segment beyond the dyad. We also defined two other collective variables based on the distance between the DNA entry and the DNA exit ends from the dyad. Although the two H3/H4 binding interfaces were theoretically identical, the asymmetry introduced by the difference in the composition of 601 DNA wrapped around the tetramer led us to distinguish between the DNA entry and AT-rich DNA exit sides of the nucleosome.

We built Markov State Models (MSMs) for nucleosome assembly under 300 mM, which was lower than the salt concentration of 400 mM used in a previous study on nucleosome assembly, due to the dramatic destabilization of our H2BK120ub system at 400 mM. We aggregated all 800 CG MD trajectories, followed by dimensionality reduction using time-lagged independent component analysis (TICA)[59] as implemented in PyEMMA 2,[60] and clustered the conformations into 400 discrete states using k-means.[61] For all systems, the MSMs were generated using a lag-time of 2×10^6 time-steps. Further increases in the lag-time did not lead to significant changes in the MSM implied time scales (Figure S11). However, the H2AK119ub and H2BK120ub systems led to faster convergence due to the higher transitions of the nucleosome to hexasomal states. Furthermore, the first two TICA coordinates were sufficient to separate the system into four regions representing the T, HR, HL, and N nucleosome states (Figure S10).

Simulation Analyses:

Root mean square deviations (RMSDs) of the ubiquitin Cα atoms were calculated using CPPTRAJ[49] after aligning the trajectories to the $(H3\text{-}H4)_2$ tetramer excluding tails. Dimer-dimer and dimer-tetramer contact analyses were conducted using the MDAnalysis package[62] and visualized using matplotlib[63], where contacts were defined between histone heavy atoms

that were within 4.5 Å of one another. The MM-GBSA (Molecular mechanics generalized born surface area) analyses were performed with igb=5 and a salt concentration of 0.15 M with the MMPBSA.py program[64]. Error bars represent the standard error of the mean, with a decorrelation time of 12.5 ns calculated by the statistical inefficiency test[65]. Generalized correlation analysis of DNA and histones were performed on C1' and Cα, respectively using correlation plus[66]. Difference maps of H2A119Kub and H2BK120ub systems were generated after subtracting from the canonical maps. Coarse-grain simulations were analyzed with in-house generated python scripts.

Results

H2AK119Ub Strengthens Ubiquitin-DNA Interactions

We conducted a series of simulations to investigate the mechanisms by which H2AK119ub and H2BK120ub affect the structure and dynamics of the nucleosomes. Specifically, we ran three replicates of 2 µs each using all-atom simulations for the canonical nucleosome core particle (NCP) and for NCPs ubiquitinated at H2AK119 (H2AK119ub) and H2BK120 (H2BK120ub) sites. In both the H2AK119ub and H2BK120ub simulations, we observed considerable movement of the ubiquitin moieties. The measurements of the root mean square deviation (RMSD) of each ubiquitin relative to the core showed displacements ranging from 15 to 50 Å in the H2AK119ub system and from 10 to 30 Å in the H2BK120ub system (Figure 2).

Analysis of ubiquitin/DNA interactions revealed different patterns based on the ubiquitination site: In the H2AK119ub system, ubiquitins interacted primarily with the entry DNA and the AT-rich exit DNA end, with the first ubiquitin binding to superhelical locations (SHL) -7.0 and the other to SHL 7.0 (Figure S2). Additionally, these ubiquitins made contacts near the DNA dyad at SHLs 0.0 and -0.5. In contrast, the H2BK120ub system showed fewer DNA contacts and differences in the SHL interaction pattern. Here, ubiquitin

on the DNA exit side (associated with H2B) did not make significant contact with DNA, while ubiquitin on the DNA entry side interacted with SHLs 3.5 and 4.0.

To assess the strength of these binding interactions, we calculated MM/GBSA-derived interaction energies between each ubiquitin and the nucleosomal DNA and histone core (Table 1). In the H2AK119ub system, the DNA entry side ubiquitin had a favorable interaction of -27.1±0.4 kcal/mol to the DNA and an unfavorable interaction of 9.2±1.1 kcal/mol to the histone core, for a total interaction of -15.9±1.1 kcal/mol. Similarly, ubiquitin at the DNA exit side had a favorable interaction energy of -19.4±kcal/mol with the DNA and an unfavorable interaction of 11.1±1.1 kcal/mol with the histone core, for a total interaction energy of -8.3±1.1 kcal/mol. Conversely, in the H2BK120ub system, the interaction energies were significantly less favorable, with the exit DNA ubiquitin having an interaction energy of -3.3±0.3 kcal/mol with the DNA and 6.7±0.3 kcal/mol with the histone core, for a total of 3.4±0.3 kcal/mol and the entry ubiquitin having DNA and histone core interactions of 7.5±0.6 and 6.2±1.0 kcal/mol, for a total interaction energy of 13.5± 1.0 kcal/mol. A decomposition of these energies into van der Waals and electrostatic components revealed that van der Waals interactions primarily facilitated ubiquitin binding, while electrostatic contributions were consistently unfavorable (Table 1). Although MM/GBSA calculations involve a number of approximations, the qualitative nature of these results is consistent with previous experimental studies, which show weak binding of ubiquitin to nucleosomal DNA.[67] Together, these findings suggest that ubiquitins on the C-terminal tails of H2A can sample more binding sites on DNA and exhibit stronger binding interactions compared to ubiquitins at H2BK120.

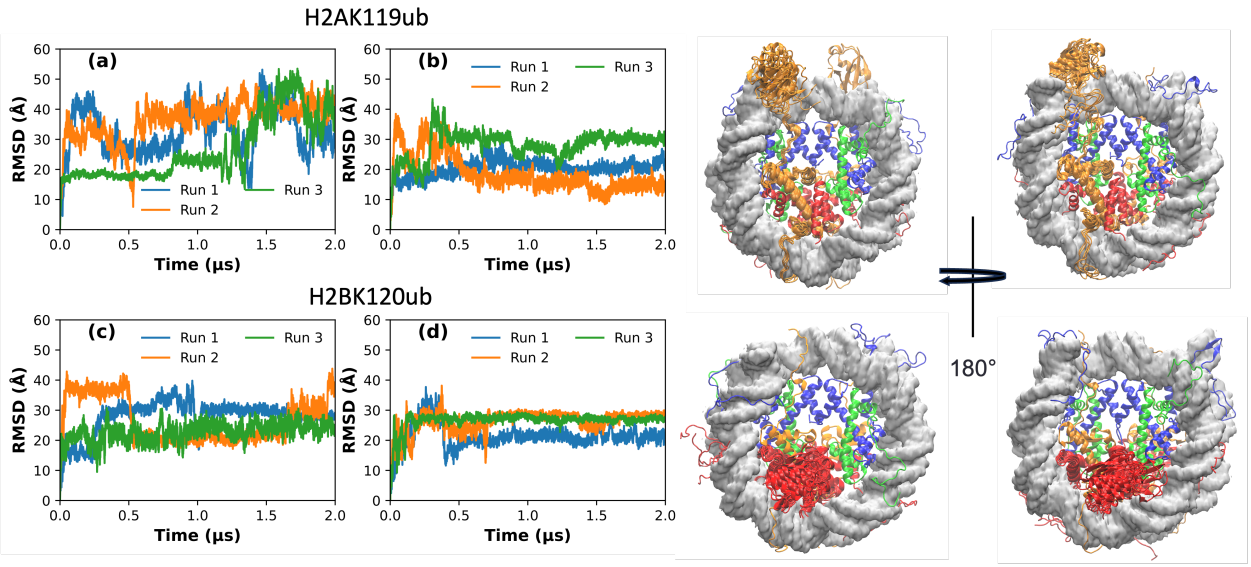

Figure 2: Root mean squared deviation of (RMSD) ubiquitin present in the H2A119Kub and H2BK120ub with ubiquitin displaying more restricted motion in H2BK120ub. Configuration of ubiquitin in top 5 clusters obtained based on the ubiquitin RMSD from the equilibrated region of the trajectories.

Ubiquitination modulates the core motions and intrinsic dynamics of H2A/H2B dimers

Having established that ubiquitin moieties undergo significant motions on the µs timescale, we sought to determine how ubiquitination affects the dynamics of the nucleosome core. To understand how these motions impact the H2A/H2B dimers, we quantified the dimer motion relative to the tetramer by defining an angle between the vectors formed by the α2 helix of H2A with the dyad axis, which corresponds to the inward and outward tilting of the H2A/H2B dimers (Figure 3). Higher tilting angles indicate outward motion of the dimer, while lower values indicate the inward motion into the core.

The mean values of this angle in the canonical system for the entry and exit side dimers were 33.8° and 34.1°, respectively. In the H2AK119ub system the DNA entry side dimer sampled values similar to the canonical, but in the DNA exit side there was an increase of ∼3°, suggesting an asymmetry in the dimer motion (Figure 3). In the H2BK120ub, system there was a statistically significant increase of 2-4° in this angle in both dimers relative to the

Table 1: MM/GBSA derived binding energies of different interacting segments in nucleosome with mean and standard error calculated across three trajectories

System	Complex	ΔE_{vdW}	ΔE_{ele}	$\Delta E_{\mathrm{total}}$
H2AK119ub	DNA-ubiquitin1	-37.5±0.1	10.4±0.4	-27.1±0.4
	DNA-ubiquitin2	-41.8±0.1	22.4±0.3	-19.4±0.3
	core-ubiquitin1	-15.8±0.1	24.0±1.1	9.2±1.1
	core-ubqiuitin2	-26.5±0.1	37.5±1.0	11.1±1.1
	dimer1-hexamer	-221.4±0.2	211.3±1.1	-10.1±1.1
	dimer2-hexamer	-222.4±0.2	207.0±0.8	-15.4±0.8
	dimer-dimer	-39.4±0.1	44.0±0.9	4.6±0.9
H2BK120ub	DNA-ubiquitin1	-10.0±0.1	6.7±0.3	-3.3±0.3
	DNA-ubiquitin2	-2.0±0.1	9.5±0.6	7.5±0.6
	core-ubiquitin1	-65.4±0.2	70.0±0.8	4.6±0.8
	core-ubiquitin2	-46.0±0.1	52.0±1.0	6.2 ±1.0
	dimer1-hexamer	-202.7±0.1	206.4±0.8	3.7±0.8
	dimer2-hexamer	-202.0±0.1	203.3±0.8	1.5±0.8
	dimer-dimer	-22.0±0.1	36.1±0.8	14.2±0.8
Canonical	dimer1-hexamer	-210.7±0.1	206.0±0.5	-4.0±0.5
	dimer2-hexamer	-208.7±0.1	210.0±0.6	1.3±0.6
	dimer-dimer	-28.2±0.1	41.5±0.8	13.2±0.8

canonical case, with values of 36.7° and 38.0°. This suggests greater outward core motions of the dimers compared to the canonical and H2AK119ub modified nucleosome. Additionally, in the canonical system, the tilting angles spanned a range of 18°, which was restricted to 12° in the H2AK119ub and H2BK120ub systems, indicating that ubiquitination may restrict dimer motions.

H2AK119Kub and H2BK120ub create opposing effects on dimer-dimer association

To further investigate the impact of system-dependent dimer motions in the histone core, we calculated the total number of contacts formed between the dimers using a distance cut-off of 4.5 Å between all heavy atoms (Figure S3). In the H2AK119ub system, the number of dimer-dimer contacts increased significantly from 51 in the canonical system to approximately 77. In contrast, in the H2BK120ub system, the number of dimer/dimer contacts was

substantially reduced to only about 34. To identify specific regions that contribute to these differences in dimer-dimer associations, we calculated per-residue contact maps (Figure 4). In the NCP, dimer-dimer interactions primarily occur through the H2A L1 and H2B L2 loops, along with the H2B α2-helix. The contact maps reveal a significant enrichment of contacts between the H2A L1-L1 and L1-H2A-α1 interfaces in H2AK119ub, while H2BK120ub shows a marked reduction in contacts at these interfaces. We observed notable rearrangements of amino acid residues at this interface in H2AK119ub, where the L1 glutamic acid formed hydrogen bond with an arginine in the H2A α1-helix of the opposing dimer. In contrast, H2BK120ub displayed a substantial loss of contacts at the dimer-dimer interface, likely due to increased outward movement and greater separation between dimers in this system. Furthermore, to probe how dimer motions affect both dimer-tetramer interactions, we analyzed the contacts formed at these interfaces. The H2AK119ub system showed a slight increase in the number of dimer/tetramer contacts, which increased from 431 to 440 for both interfaces, while in the H2BK120ub system contacts were reduced to 425 and 421, which was lower than both the canonical and H2AK119ub systems, suggesting that ubiquitination had opposite affect on these interfaces (Figure S4).

The impact of these changes on each dimer's stability in the histone core was assessed with MM/GBSA calculations between each dimer and the remaining hexamer. These calculations revealed a significant increase in net van der Waals (vdW) interaction energies in H2AK119ub, resulting in more favorable total interaction energies than in the canonical NCP, with total ΔE values of -10.1±1.1 kcal/mol and -15.4±0.8 kcal/mol for the DNA entry and AT-rich DNA exit dimers, respectively. In contrast, MM/GBSA analysis for H2BK120ub indicated a net unfavorable ΔE binding of dimers in the histone core, with values of 3.7±0.8 kcal/mol and 1.5±0.8 kcal/mol, suggesting reduced dimer association stability in the H2BK120ub system.

To understand the effects of ubiquitination on DNA dynamics, we examined DNA base-pair unwrapping along the superhelical axis over the course of our 2.0 µs simulations (Figure

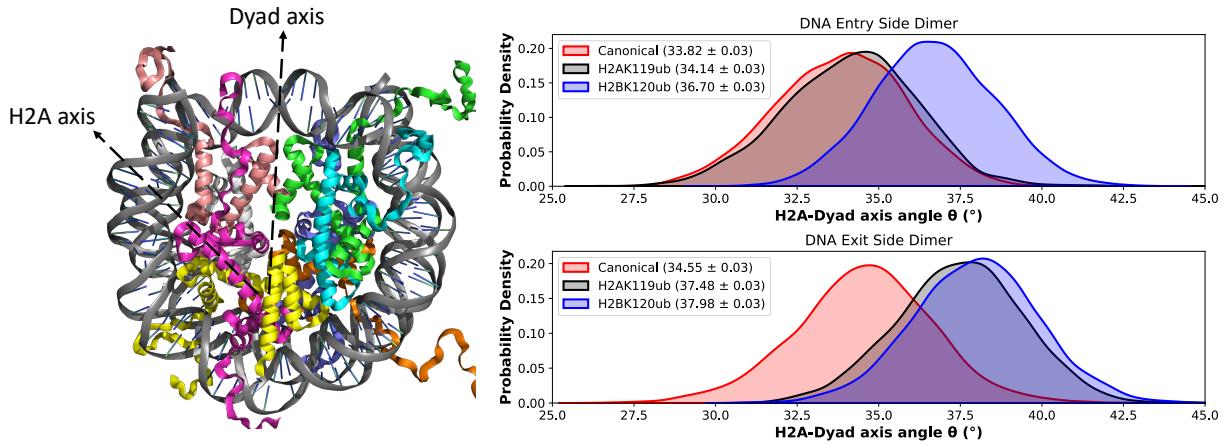

Figure 3: Depiction of Dyad axis and H2A axis angle. The distribution and the mean of H2A-dyad angle representing the higher outward tilting of the dimers.

5). In the canonical system, unwrapping of the entry DNA was observed in a single trajectory, where four to eight base pairs were unwrapped after 1.0 µs, while the exit side of the DNA showed only the transient unwrapping of up to four basepairs in each trajectory. In the H2BK120ub system, there was unwrapping of around four basepairs from the entry DNA and ten from the exit side in the first trajectory, with little to no unwrapping in the other simulations. In contrast, in the H2AK119ub system, there was only slight unwrapping in a single trajectory which briefly exceeded four basepairs, with no unwrapping observed in the other trajectories. Together, these results suggest that H2AK119ub stabilizes DNA wrapping relative to the canonical and H2BK120 states, likely due to additional interactions introduced by ubiquitin at the entry and exit sites, which help maintain a more compact structure.

In addition to impacting dimer and DNA structures and dynamics, ubiquitination also affected local and long-range dynamic correlations throughout the NCP (Figure S5). Mutual information calculations of the protein Cα and DNA C1' atom dynamics in the canonical system show high correlation between histone-histone and histone-DNA components. Inter-subunit correlations, represented by off-diagonal blocks in the correlation matrices, remained lower for ubiquitinated states and were drastically reduced in the H2BK120ub system. Cor-

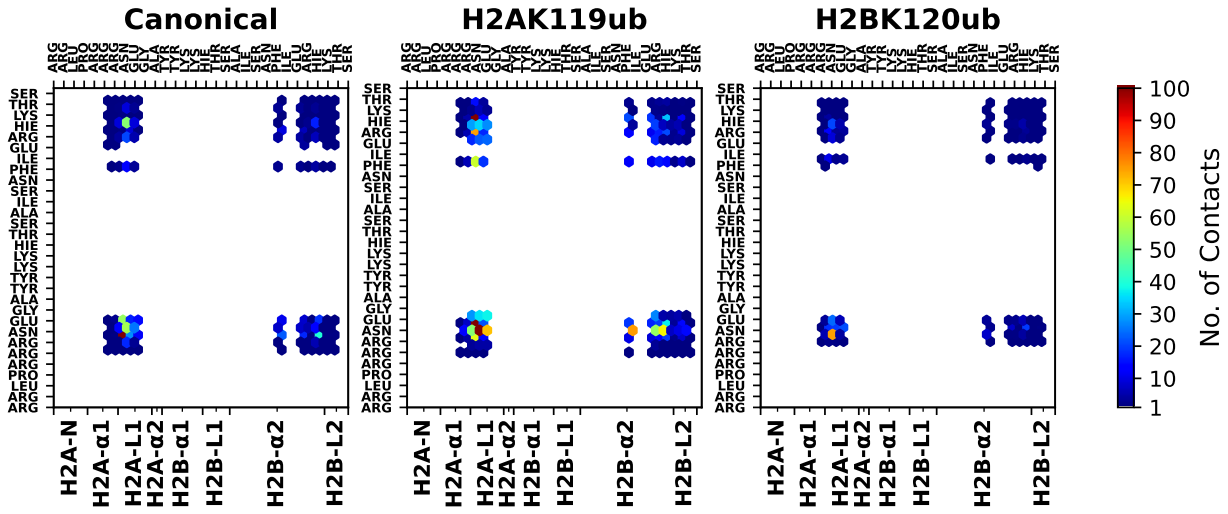

Figure 4: Contact maps representing the number of per-residue contacts at dimer-dimer interacting interfaces in all the systems with the colorbar representing the total number of contacts

relation differences relative to the canonical system show a disparate impact on system correlations from H2AK119ub and H2BK120ub ubiquitination. In the H2AK119ub system, the first dimer had relatively small increases in correlation (on the order of 0.05-0.10) with the tetramer and DNA, while the DNA exit dimer had lower correlations with the entire NCP (Figure 6a). In contrast, in the H2BK120ub system, both exit and entry dimers showed a decoupling between the dynamics of the H2A and H2B monomer, along with a greater reduction in the H2B correlations with the other histones and DNA (Figure 6b). At the same time, the N-terminus of the H3 and H4 histones exhibited higher correlations with the other histones and DNA. In general, the changes introduced in the H2BK120ub correlations were larger in magnitude than those in the H2AK119ub system, with multiple correlation changes in the range of 0.15-0.20 compared to the more typical values of 0.05 in H2AK119ub. Together, correlation analyses show that ubiquitination had a site-dependent effect on modulating the inter- and intra-nucleosome dynamics, with H2BK120ub having a larger magnitude effect than H2AK119ub.

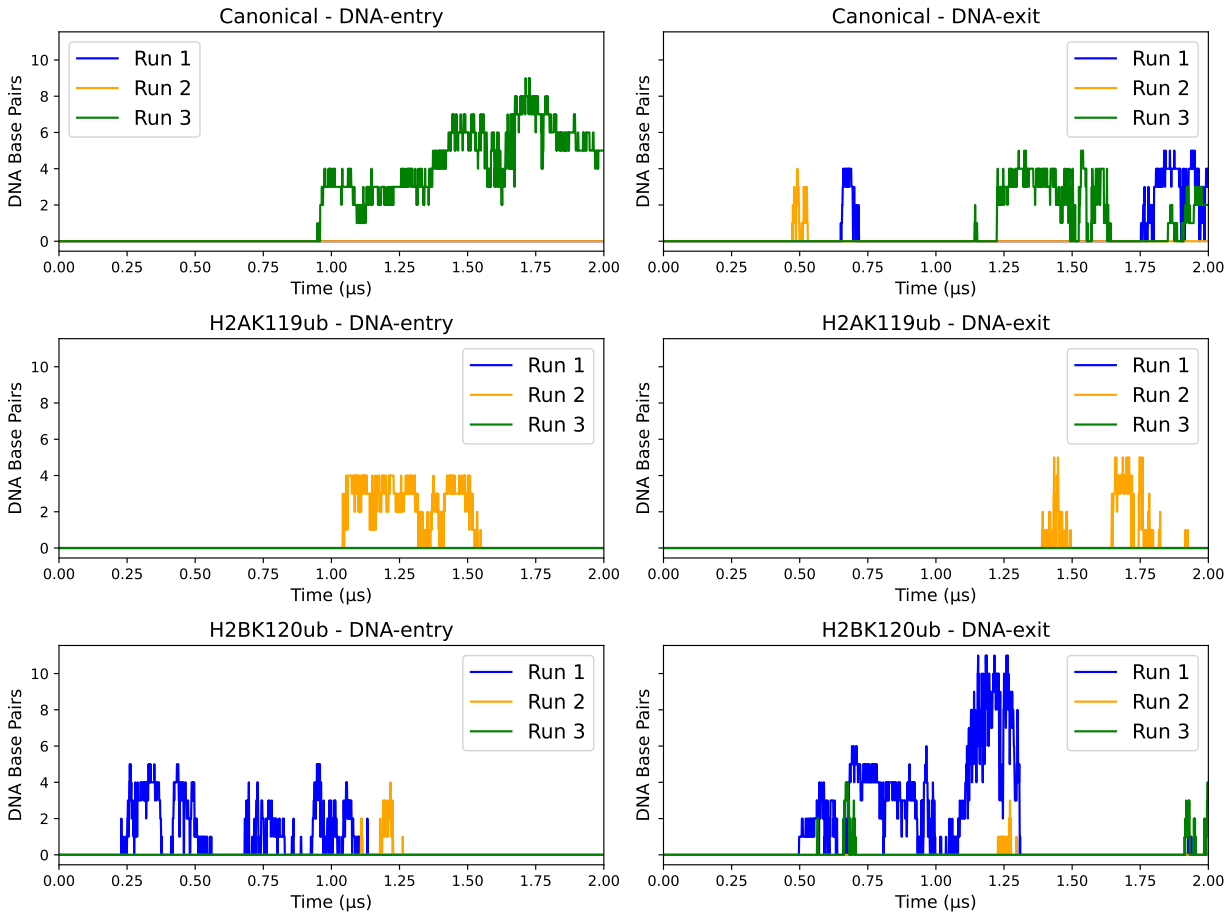

Figure 5: Unwrapping of exit and entry side DNA the histone core in all the systems.

Nucleosome folding is favored from the DNA exit folded hexasome and on pathway intermediates from open tetrasomal states.

All-atom simulations revealed that both ubiquitinations influenced nucleosome structures and dynamics on the microsecond timescale. H2AK119ub stabilized nucleosome dynamics where ubiquitin directly interacts with DNA and also strengthens the association of dimers in the histone core, whereas H2BK120ub reduced the stability of dimers in the histone core and increased overall dynamics of the nucleosome. We hypothesized that all-atom nucleosome dynamics differences observed accross systems could affect large-scale structural variations such as folding of nucleosomes over longer timescales, which were not accessible due to the high computational cost of all-atom simulations. Therefore, we performed a series of

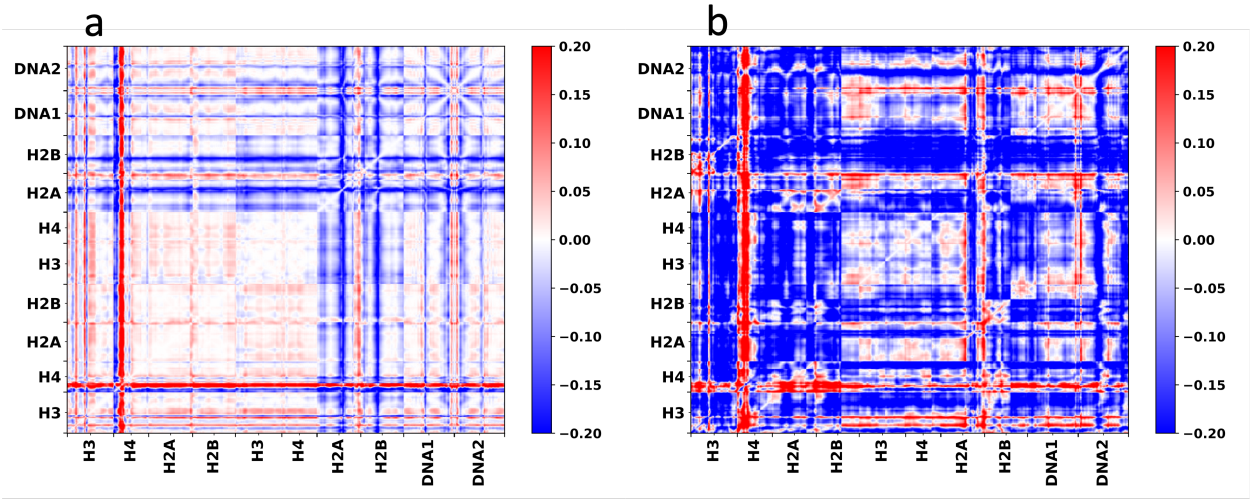

Figure 6: Difference between atomic mutual information in ubiquitinated and canonical states. Negative values represent decrease in coupled motions, whereas positive values indicates increase in coupled motions relative to the canonical state. Blocks along the diagonal intra-correlations in histones and DNA. Non-diagonal blocks represent the histone-histone and histone-DNA correlations.

coarse grain simulations on canonical nucleosomes, H2AK119ub, and H2BK120ub. These simulations utilized the 3SPN.2C[51] DNA and AICG2+ structure-based protein potentials, with the ubiquitin linkage parameterized using iterative Boltzmann inversion simulations (Figure S9) following the work of Terakawa and Takada.[55] For each system, 800 simulations of 10^8 steps were performed from nucleosomal, hexasomal, and tetrasomal states, and the results were integrated into a Markov State Model (MSM) (see Methods for more details).

The MSM for the canonical NCP was clustered into 11 macrostates. For clarity, a model with the six maximum flux pathways from the tetrasomal to nucleosomal states is shown in Figure 7, while the complete MSM with all transition probabilities is presented in Figure S6. We identified three dominant tetrasomal states (T, T1, T2) which differed in the degree of DNA extension and the positioning of the H2A/H2B dimers. State T shows fully extended DNA arms with one H2A/H2B dimer located at the ends and the other closer to the tetramer. In contrast, T2 adopted a more compact form, with the dimer bound DNA arms closer together and nearer to the core and bending of DNA around one of the dimers. T1 represents the most compact state, with the dimers nestled between the two DNA strands. In addition,

there were four prominent hexasomal states, which we label HR, HR2, HR3, and HL. In HR, the dimer bound close to the core, and the unwrapped AT-poor side of the DNA entry strand, while in HR1 the dimer was positioned at the DNA end, suggesting nonspecific DNA/dimer interactions. In HL, the AT rich DNA exit strand is unwrapped along with the dimer. Finally, there was one dominant nucleosome state, denoted as N.

The state free energies showed that the nucleosomal state was the most dominant, with the highest MSM population and the lowest free energy. However, other macrostates had relatively low free energies, suggesting that they are marginally populated at room temperature. For example, the hexasomal state (HR) had a free energy of only 0.25 kcal/mol above the nucleosomal state, while the HR2, HR3 and HL states had higher free energies of 2.18-3.05 kcal/mol. This points towards the HR state as being the dominant hexasomal conformation. In contrast, all three tetrasomal states had nearly the same free energies of 1.29-1.57 kcal/mol above the nucleosomal state despite their varying degrees of compactness. Together, this suggests that the canonical coarse-grain system can exist in a population of states with various degrees of compactness and DNA wrapping.

An analysis of the pathways from the tetrasomal to the haxasomal states demonstrates that the dominant folding pathway follows the T-T2-HR-N states. This pathway includes first folding of the open tetrasome (T) to compact tetrasomal states (T2), followed by a transition to the low free energy HR hexasome state, before folding to the nucleosome state. The total mean first passage time (MFPT) of this pathway is $3.83{\cdot}10^9$ MD steps, and encompasses 51.6% of the total flux between the tetrasomal and nucleosomal states (Table 3). The second dominant pathway bypassed the HR state and proceeded through folding of the open tetrasomal state into the HL hexasome, which then transitioned to H3, then to HR2, before finally folding into the nucleosome. This pathway had an MFPT an order of magnitude higher than the first pathway ($1.19{\cdot}10^{10}$) and encompassed 16.6% of the total flux. The third dominant folding pathway was similar to the first; however, the folding between the T and T2 tetrasomal states was not direct and instead went through the compact T1 state.

This increased the MFPT to $2.09 \cdot 10^{10}$ steps and represented 9.5% of the total flux. One of the most important features which emerged from this analysis is the unraveling of the DNA entry side causing the enrichment of HR states in the folding pathways, which is in line with the higher breathing from the DNA entry side in all-atom simulations. In general, pathway analysis indicates that the folding from the tetrasomal to nuclesomal states is dominated by a small number of pathways that proceed through states that sequentially compact the histone core.

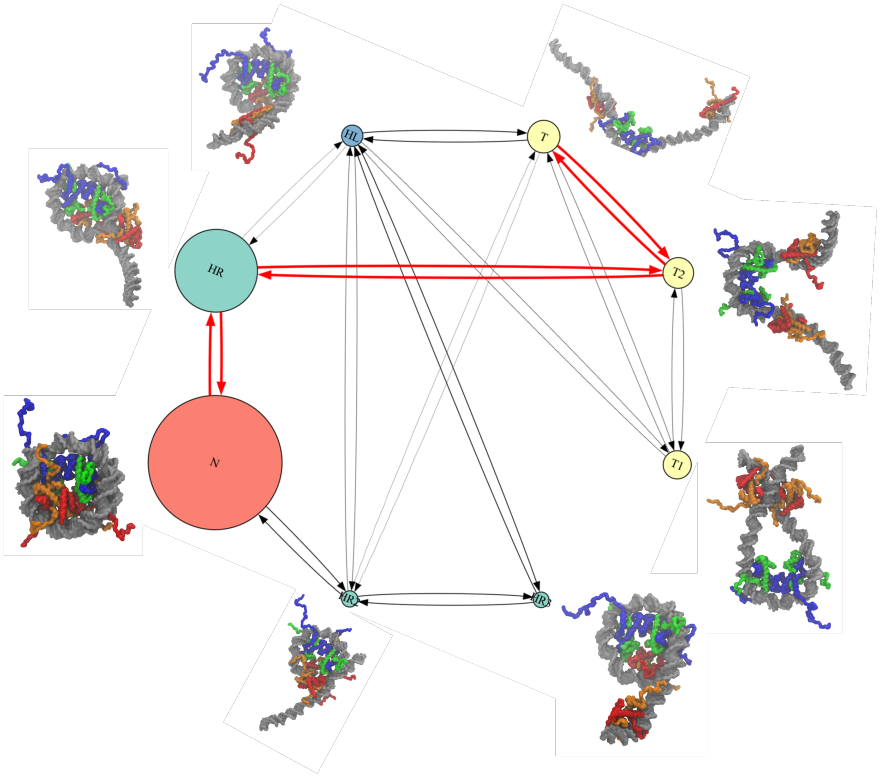

Figure 7: The top 6 pathways of canonical nucleosome assembly were identified using transition path theory. Each node represents the state and sized by the equilibrium free energy. The arrow thickness represents the dominance of the pathway. States and their energies relative to the most probable state are given in a tabular format.

Table 2: Energy states of nucleosome dynamics.

State	**Kcal/mol**
Tetrasome (extended),	T (1.29), T2 (1.40)
Tetrasome (Compact)	T1 (1.57)
Hexasome Right (HR) - DNA-exit-side folded	HR (0.25), HR2 (3.04), HR3 (3.06)
Hexasome Left (HL) - DNA-entry-side folded	HL (2.18)
Nucleosome (N)	N (0.00)

Table 3: Pathways and Mean First Passage Time of Canonical system

Rank	Pathway	Mean First Passage Time	% of Total Flux
1	T-T2-HR-N	$3.83 \cdot 10^{9}$	51.6%
2	T-HL-HR3-HR2-N	$1.19 \cdot 10^{10}$	16.6%
3	T-T1-T2-HR-N	$2.09 \cdot 10^{10}$	9.5%
4	T-T1-HL-HR1-N	$2.09 \cdot 10^{10}$	9.4%
5	T-HR1-N	$5.31 \cdot 10^{10}$	3.7%
6	T-T1-HL-HR-N	$5.37 \cdot 10^{10}$	2.1%

Ubiqutination destabilizes nucleosomal states and increases folding times

To understand how ubiquitination affects large-scale nucleosome structures, similar coarse-grain simulations and Markov State Models were computed for H2AK119 and H2BK120 ubiquinated nucleosomes. In general, the conformations of macrostates identified in these analyses were similar to those in the canonical system, however the free energies of these states, and the transitions between them, were significantly affected by ubiquitination.

In the H2AK119 ubiquitinated system, the nucleosomal state was significantly destabilized compared to the tetrasomal states. Indeed, the extended tetrasomal states T and T1 had free energies of 0.00 and 0.64 kcal/mol, whereas the more compact tetrasomal states T2 and Part_T had similar low free energies of 0.36 and 0.87 kcal/mol (Table 5). In contrast, the nucleosomal state had a free energy of 6.54 kcal/mol. The hexasomal states all had free energies in the 5.70-6.12 kcal/mol range, with the exception of the HL1 state, which had a free energy of 0.95 kcal/mol.

The folding pathways for the H2AK119ub system were slower than those in the canonical state, and although there were slightly more folding pathways with significant flux, there were still only a handful of pathways between the tetrasomal and nucleosomal states. The two fastest folding pathways had nearly identical MFPTs of around $9.0 \cdot 10^{10}$ timesteps, each representing 24.7% and 24.3% of the total flux, respectively. The first pathway transitioned from the extended T to T1 tetrasome states, and folded into the left hexasomeme states HL1 and H1 before folding into the N nucleosome state. The second pathway was similar, however instead of folding through the HL1 state in folding through the tetrasomsal Part_T state. Pathways three through five also had significant flux (11.7%-16. 0%) with MFPT ranging from $1.37 \cdot 10^{11}$-$1.87 \cdot 10^{11}$ timesteps.

Table 4: Pathways and Mean First Passage Time of H2AK119ub system

Rank	Pathway	Mean First Passage Time	% of Total Flux
1	T-T1-HL1-HL-N	$8.86*10^{10}$	24.7%
2	T-T1-Part_T-HL-N	$9.00*10^{10}$	24.3%
3	T-T1-T2-Part_T-HL1-HL-N	$1.37*10^{11}$	16.0%
4	T-Part_T-HR-N	$1.47*10^{11}$	15%
5	T-T1-T2-Part_T-HR1-HR-N	$1.87*10^{11}$	11.7%
6	T-HL1-HL-N	$4.86*10^{11}$	4.5%

Table 5: Energy of nucleosomal states in H2AK119ub.

State	**Energy (Kcal/mol)**
Tetrasome (Extended)	T (0.64), T1 (0.00),
Tetrasome (Compact)	T2 (0.36), Part_T (0.87)
Hexasome Right (HR) - DNA-exit-side folded	HR (6.12), HR1 (6.11)
Hexasome Left (HL) - DNA-entry-side folded	HL (5.70), HL1 (0.95)
Nucleosome (N)	N (6.54)

Ubiquitination at H2BK120 resulted in further destabilization of the nucleosomal state. In the H2KB120ub MSM the nucleosome was sparsely populated, with a free energy of 10.01 kcal/mol. There were multiple extended and compact tetrasomal states, all of which had low free energies ranging from 0.00 to 1.49 kcal/mol. Two hexasomal states were observed,

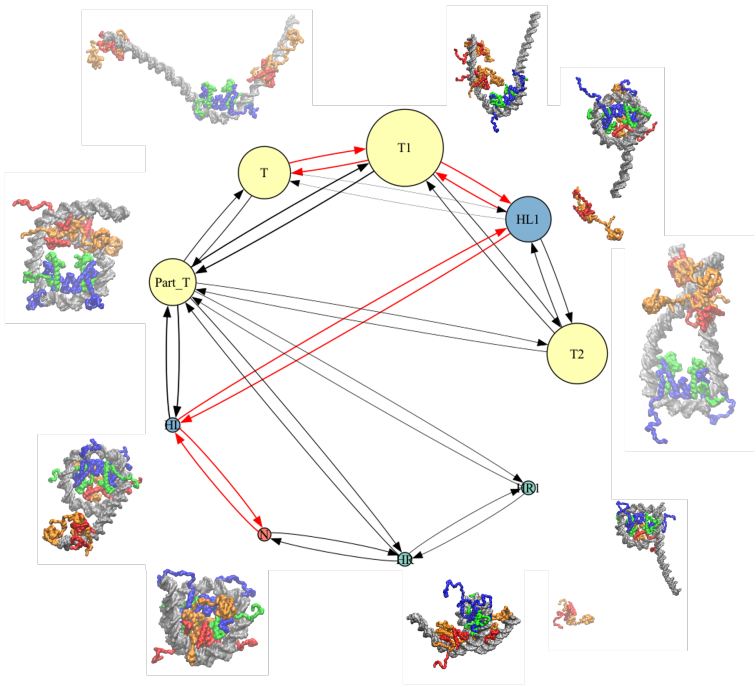

Figure 8: The top 6 pathways of H2A119Kub modified nucleosome assembly were identified using transition path theory. Each node represents the state and sized by the equilibrium free energy. The arrow thickness represents the dominance of the pathway. States and their energies relative to the most probable state are given in a tabular format.

one with the hexamer on the entry DNA and the other on the exit DNA. In both cases, the free energy was between the tetramer and nucleosome states at 3.28 kcal/mol (Table 7).

The pathway to nucleosome assembly in the H2BK120ub system was more diffuse with numerous interconnected states than in the canonical or H2AK119ub systems (Figures 9 and S8). The folding times were also significantly slower: the fastest MFPT was $5.03{\cdot}10^{11}$ steps, two and one order of magnitude greater than the canonical and H2AK119ub systems, respectively (Table 6). Although both the HL and HR states had similar free energies, the first three dominant pathways all transitioned from the tetrasomal to the nucleosome state through HL. However, given that the dominant pathway only represents 0.3% of the total flux from the tetrasome to the nucleosome, the H2BK120 folding mechanism is highly heterogeneous when it occurs, a marked contrast to the canonical and H2AK119ub states.

Table 6: Pathways and Mean First Passage Time of H2BK120ub system

Rank	Pathway	Mean First Passage Time	% of Total Flux
1	T-T1-HL-N	$5.03*10^{11}$	0.3%
2	T-Part_T-HL-N	$8.61*10^{11}$	0.2%
3	T-Part_T-T1-HL-N	$9.80*10^{11}$	0.2%
4	T-HR-N	$1.58*10^{12}$	0.1%
5	T-T2-T5-T4-HL-N	$2.32*10^{12}$	0.1%
6	T-T3-HR-HL-N	$2.55*10^{12}$	0.1%

Table 7: Energy of nucleosomal states in H2BK119ub.

State	**Energy (Kcal/mol)**
Tetrasome (Extended)	T (1.10), T2 (0.51), T5(0.00)
Tetrasome (Compact)	Part_T(1.13), T1 (0.78), T3 (1.49), T4 (1.13)
Hexasome Right (HR) - DNA-exit-side folded	HR (3.28)
Hexasome Left (HL) - DNA-entry-side folded	HL (3.28)
Nucleosome (N)	N (10.01)

Discussion

Ubiquitination of histones at specific sites, such as H2AK119 and H2BK120, correlates with either inactive or active chromatin states[23,25], respectively. Experimental studies have shown that ubiquitin can affect nucleosome stability[68]. However, the precise structural mechanisms by which ubiquitin modulates nucleosome dynamics remains unclear. In this study, we employed both all-atom and coarse-grain simulations to investigate the effects of ubiquitin on nucleosome dynamics over microsecond and millisecond timescales, respectively, which are relevant for nucleosome assembly.

Our results indicate that ubiquitination modulates histone dimer motions within the histone core. In the H2BK120ub system, both H2A/H2B dimers exhibited a pronounced outward tilting motion relative to the dyad axis. In the H2AK119ub system, this effect was asymmetric, where the motion of one dimer remained similar to that of the canonical system, while the other dimer sampled higher tilting angles similar to the H2BK120ub system over

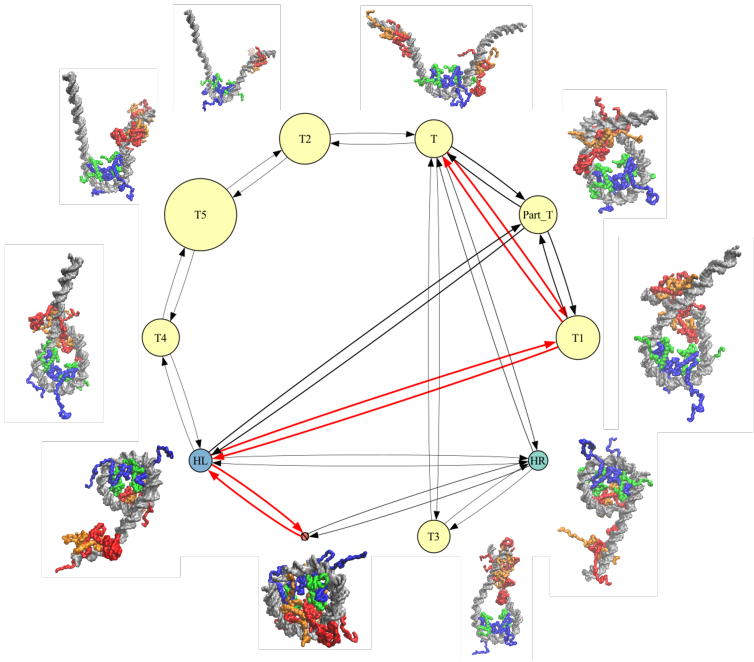

Figure 9: The top 6 pathways of H2BK120 modified nucleosome assembly were identified using transition path theory. Each node represents the state and sized by the equilibrium free energy. The arrow thickness represents the dominance of the pathway. States and their energies relative to the most probable state are given in a tabular format.

the course of 2 µs (Figure 3).

In particular, ubiquitination affects contacts at the H2A L1-L1 interface, a region of the nucleosome that has been directly implicated in overall nucleosomal stability.[69,70] The H2A L1 loops are comprised of four residues located at the base of the nucleosome near SHLs ±4, and the interaction between the two H2A L1 loops are the only points of contact between the two dimers. Indeed, changes in the L1-L1 interface in histone variants such as macroH2A variants have been shown to result in more or less stable nucleosomes[70,71]. Our simulation show that ubiquitination at the H2BK120 site significantly disrupts these L1-L1 interface contacts, while ubiquitination at H2AK119 reorganized the L1-L1 interface and enhances both these dimer-dimer as well as other dimer-tetramer contacts (Figures S3 and S4). This weakening of contacts is likely a cause of the significant decoupling of motions observed in H2BK120ub nucleosomes between the dimers, the tetramer, and the nucleosomal DNA (Figure 6), and in both systems it may contribute to the observed increase in dimer

orientations relative to the canonical nucleosome.

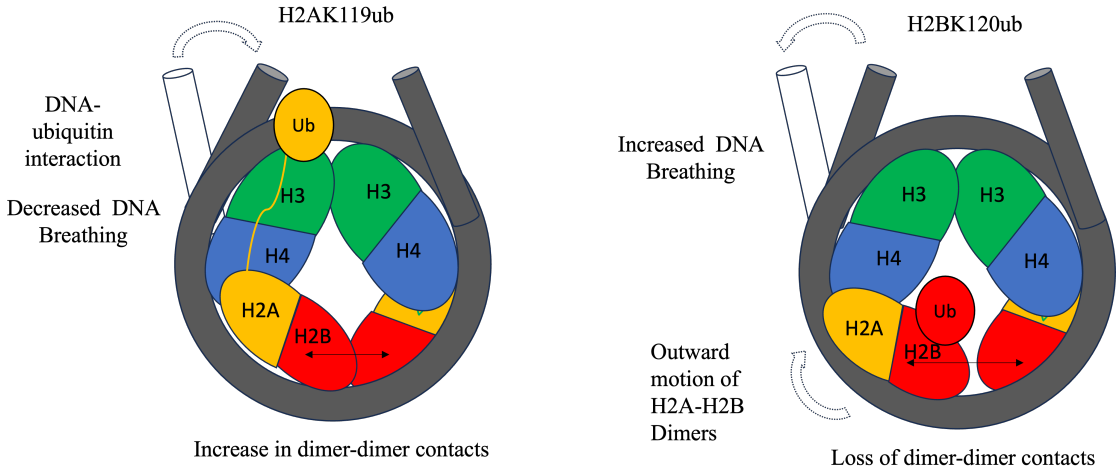

Figure 10: Cartoon illustration highlighting the structural basis of ubquitin induced changes in the nucleosomal dynamics.

Our coarse-grain simulations, which were similar to experiments in which the H2A/H2B dimers were introduced into pre-formed tetrasomal states[25,58], demonstrate that while the ubiquitin does not alter the overall folding patterns of the nucleosome from tetramer to hexasomal to nucleosomal states, it substantially slows the process. Specifically, H2AK119ub slows nucleosome folding by an order of magnitude (Table 4), whereas H2BK120ub causes an even more pronounced reduction of two orders of magnitude (Table 6). Additionally, in both ubiquitinated systems the nucleosomal states were destabilized and the hexasomal states were energetically more favorable than the fully formed nucleosomes (Tables 5 and 7). For instance, in the canonical case the most stable hexasomal state has roughly similar free energy to the hexasome, whereas in H2AK119ub and H2BK120ub the most stable hexasomal states are approximately 6 kcal/mol more favorable than their nucleosomal counterparts. Furthermore, in both cases, the tetrasomal states are the most energetically favored. This significant energy difference highlights a shift in the equilibrium, favoring the tetrasomal and hexasomal states in ubiquitinated systems.

The conclusion that di-ubiquitination destabilizes the nucleosome and creates more dynamic nucleosomal states relative to the canonical nucleosome is in accord with recent single-

molecule experiments. In work by Luo *et al.*, single-molecule magnetic tweezer experiments showed that monoubiquintated H2BK120 nucleosomes have lower mechanical stability than their canonical counterparts, which increases the affinity of the FACT complex to maintain transcriptionally active state.[25] In addition, Luo *et al.* observed that the free energy of unwrapping the outer fold of DNA was on the order of 5 kcal/mol, which is similar to the free energy differences observed between the hexasomal and tetrasomal states in our MSM calculation. Although this work focused on monoubiquitinated nucleosomes, one would expect a similar, if not enhanced effect in di-ubiquitinated systems.

Although the simulations employed here were designed to sample both short and long-timescales, it should be noted that the coarse-graining approach has several limitations that may impact their accuracy. For example, it is a simplified model in which the ionic atmosphere is approximated with a Debye–Hückel formalism[72]. It also does not capture secondary structure changes and relies on native-contacts, some of which our all-atom simulations showed were disrupted on the microsecond timescale. Although these limitations should be taken into account when accessing the overall numerical accuracy of the resulting MSMs, similar models have shown good agreement with experimental results[73,74], indicating that they are reliable for generating biophysical insights into these and similar systems.

Overall, our study provides a structural framework for understanding how ubiquitination at H2A119Ub and H2BK120Ub exerts opposing effects on nucleosome dynamics, emphasizing that ubiquitination is not merely an epigenetic mark but also a key regulator of chromatin's physical properties. While our findings offer critical mechanistic insights, experimental validation will be necessary to determine how these modifications influence higher-order chromatin folding and gene regulation. Integrating computational and experimental approaches will be essential for uncovering the broader principles by which ubiquitination modulates chromatin architecture and function.

Data availability

MD trajectories generated in this study are available on Zenodo at: `https://doi.org/10.5281/zenodo.14866729`

References

(1) Luger, K.; Mäder, A. W.; Richmond, R. K.; Sargent, D. F.; Richmond, T. J. Crystal structure of the nucleosome core particle at 2.8 Å resolution. *Nature* **1997**, *389*, 251–260.

(2) McGinty, R. K.; Tan, S. Nucleosome structure and function. *Chemical reviews* **2015**, *115*, 2255–2273.

(3) Bilokapic, S.; Strauss, M.; Halic, M. Histone octamer rearranges to adapt to DNA unwrapping. *Nature structural & molecular biology* **2018**, *25*, 101–108.

(4) Mariño-Ramírez, L.; Kann, M. G.; Shoemaker, B. A.; Landsman, D. Histone structure and nucleosome stability. *Expert review of proteomics* **2005**, *2*, 719–729.

(5) Peng, Y.; Li, S.; Landsman, D.; Panchenko, A. R. Histone tails as signaling antennas of chromatin. *Current opinion in structural biology* **2021**, *67*, 153–160.

(6) Karantza, V.; Freire, E.; Moudrianakis, E. N. Thermodynamic studies of the core histones: pH and ionic strength effects on the stability of the (H3- H4)/(H3- H4) 2 system. *Biochemistry* **1996**, *35*, 2037–2046.

(7) Hazan, N. P.; Tomov, T. E.; Tsukanov, R.; Liber, M.; Berger, Y.; Masoud, R.; Toth, K.; Langowski, J.; Nir, E. Nucleosome core particle disassembly and assembly kinetics studied using single-molecule fluorescence. *Biophysical journal* **2015**, *109*, 1676–1685.

(8) Weaver, T. M.; Morrison, E. A.; Musselman, C. A. Reading more than histones: the prevalence of nucleic acid binding among reader domains. *Molecules* **2018**, *23*, 2614.

(9) Isaac, R. S.; Jiang, F.; Doudna, J. A.; Lim, W. A.; Narlikar, G. J.; Almeida, R. Nucleosome breathing and remodeling constrain CRISPR-Cas9 function. *Elife* **2016**, *5*, e13450.

(10) Widom, J. Structure, dynamics, and function of chromatin in vitro. *Annual review of biophysics and biomolecular structure* **1998**, *27*, 285–327.

(11) Huertas, D.; Sendra, R.; Muñoz, P. Chromatin dynamics coupled to DNA repair. *Epigenetics* **2009**, *4*, 31–42.

(12) Millán-Zambrano, G.; Burton, A.; Bannister, A. J.; Schneider, R. Histone post-translational modifications—cause and consequence of genome function. *Nature Reviews Genetics* **2022**, *23*, 563–580.

(13) Bowman, G. D.; Poirier, M. G. Post-translational modifications of histones that influence nucleosome dynamics. *Chemical reviews* **2014**, *115*, 2274–2295.

(14) Chen, J. J.; Stermer, D.; Tanny, J. C. Decoding histone ubiquitylation. *Frontiers in Cell and Developmental Biology* **2022**, *10*, 968398.

(15) Zhang, Y. Transcriptional regulation by histone ubiquitination and deubiquitination. *Genes & development* **2003**, *17*, 2733–2740.

(16) Goldknopf, I. L.; Busch, H. Isopeptide linkage between nonhistone and histone 2A polypeptides of chromosomal conjugate-protein A24. *Proceedings of the National Academy of Sciences* **1977**, *74*, 864–868.

(17) Weake, V. M. Histone ubiquitylation control of gene expression. *Fundamentals of Chromatin* **2013**, 257–307.

(18) Meas, R.; Mao, P. Histone ubiquitylation and its roles in transcription and DNA damage response. *DNA repair* **2015**, *36*, 36–42.

(19) Nathan, D.; Ingvarsdottir, K.; Sterner, D. E.; Bylebyl, G. R.; Dokmanovic, M.; Dorsey, J. A.; Whelan, K. A.; Krsmanovic, M.; Lane, W. S.; Meluh, P. B.; others Histone sumoylation is a negative regulator in Saccharomyces cerevisiae and shows dynamic interplay with positive-acting histone modifications. *Genes & development* **2006**, *20*, 966–976.

(20) Wang, H.; Zhai, L.; Xu, J.; Joo, H.-Y.; Jackson, S.; Erdjument-Bromage, H.; Tempst, P.; Xiong, Y.; Zhang, Y. Histone H3 and H4 ubiquitylation by the CUL4-DDB-ROC1 ubiquitin ligase facilitates cellular response to DNA damage. *Molecular cell* **2006**, *22*, 383–394.

(21) Shafiq, T. A.; Yu, J.; Feng, W.; Zhang, Y.; Zhou, H.; Paulo, J. A.; Gygi, S. P.; Moazed, D. Genomic context–and H2AK119 ubiquitination–dependent inheritance of human Polycomb silencing. *Science Advances* **2024**, *10*, eadl4529.

(22) Oss-Ronen, L.; Sarusi, T.; Cohen, I. Histone mono-ubiquitination in transcriptional regulation and its mark on life: emerging roles in tissue development and disease. *Cells* **2022**, *11*, 2404.

(23) Tamburri, S.; Lavarone, E.; Fernández-Pérez, D.; Conway, E.; Zanotti, M.; Manganaro, D.; Pasini, D. Histone H2AK119 mono-ubiquitination is essential for polycomb-mediated transcriptional repression. *Molecular cell* **2020**, *77*, 840–856.

(24) Ciapponi, M.; Karlukova, E.; Schkölziger, S.; Benda, C.; Müller, J. Structural basis of the histone ubiquitination read–write mechanism of RYBP–PRC1. *Nature Structural & Molecular Biology* **2024**, 1–5.

(25) Luo, A.; Kong, J.; Chen, J.; Xiao, X.; Lan, J.; Li, X.; Liu, C.; Wang, P. Y.; Li, G.; Li, W.; Chen, P. H2B ubiquitination recruits FACT to maintain a stable altered nucleosome state for transcriptional activation. *Nat Commun* **2023**, *14*, 741.

(26) Xiao, X.; Liu, C.; Pei, Y.; Wang, Y.-Z.; Kong, J.; Lu, K.; Ma, L.; Dou, S.-X.; Wang, P.-Y.; Li, G.; others Histone H2A ubiquitination reinforces mechanical stability and asymmetry at the single-nucleosome level. *Journal of the American Chemical Society* **2020**, *142*, 3340–3345.

(27) Miyagi, A.; Ando, T.; Lyubchenko, Y. L. Dynamics of nucleosomes assessed with time-lapse high-speed atomic force microscopy. *Biochemistry* **2011**, *50*, 7901–7908.

(28) van Deelen, K.; Schiessel, H.; de Bruin, L. Ensembles of breathing nucleosomes: a computational study. *Biophysical Journal* **2020**, *118*, 2297–2308.

(29) Woods, D. C.; Wereszczynski, J. Elucidating the influence of linker histone variants on chromatosome dynamics and energetics. *Nucleic acids research* **2020**, *48*, 3591–3604.

(30) Armeev, G. A.; Kniazeva, A. S.; Komarova, G. A.; Kirpichnikov, M. P.; Shaytan, A. K. Histone dynamics mediate DNA unwrapping and sliding in nucleosomes. *Nature communications* **2021**, *12*, 2387.

(31) Brandani, G. B.; Tan, C.; Takada, S. The kinetic landscape of nucleosome assembly: A coarse-grained molecular dynamics study. *PLoS computational biology* **2021**, *17*, e1009253.

(32) Portillo-Ledesma, S.; Tsao, L. H.; Wagley, M.; Lakadamyali, M.; Cosma, M. P.; Schlick, T. Nucleosome clutches are regulated by chromatin internal parameters. *Journal of Molecular Biology* **2021**, *433*, 166701.

(33) Li, S.; Wei, T.; Panchenko, A. Histone variant H2A. Z modulates nucleosome dynamics to promote DNA accessibility. *Biophysical Journal* **2023**, *122*, 218a.

(34) Patel, R.; Onyema, A.; Tang, P. K.; Loverde, S. M. Conformational Dynamics of the Nucleosomal Histone H2B Tails Revealed by Molecular Dynamics Simulations. *Journal of Chemical Information and Modeling* **2024**,

(35) Fedulova, A. S.; Armeev, G. A.; Romanova, T. A.; Singh-Palchevskaia, L.; Kosarim, N. A.; Motorin, N. A.; Komarova, G. A.; Shaytan, A. K. Molecular dynamics simulations of nucleosomes are coming of age. *WIREs Computational Molecular Science* **2024**, *14*, e1728.

(36) Kariyawasam, N. L.; Wereszczynski, J. The Influence of Ionic Environment on Nucleosome–Mica Interactions Revealed via Molecular Dynamics Simulations. *The Journal of Physical Chemistry B* **2024**, *128*, 12038–12049.

(37) Husic, B. E.; Pande, V. S. Markov state models: From an art to a science. *Journal of the American Chemical Society* **2018**, *140*, 2386–2396.

(38) Davey, C. A.; Sargent, D. F.; Luger, K.; Maeder, A. W.; Richmond, T. J. Solvent mediated interactions in the structure of the nucleosome core particle at 1.9 Å resolution. *Journal of molecular biology* **2002**, *319*, 1097–1113.

(39) Pettersen, E. F.; Goddard, T. D.; Huang, C. C.; Couch, G. S.; Greenblatt, D. M.; Meng, E. C.; Ferrin, T. E. UCSF Chimera—a visualization system for exploratory research and analysis. *Journal of computational chemistry* **2004**, *25*, 1605–1612.

(40) Widom, J. Role of DNA sequence in nucleosome stability and dynamics. *Quarterly reviews of biophysics* **2001**, *34*, 269–324.

(41) Frisch, A.; others gaussian 09W Reference. *Wallingford, USA, 25p* **2009**, *470*.

(42) Tian, C.; Kasavajhala, K.; Belfon, K. A.; Raguette, L.; Huang, H.; Migues, A. N.; Bickel, J.; Wang, Y.; Pincay, J.; Wu, Q.; others ff19SB: amino-acid-specific protein backbone parameters trained against quantum mechanics energy surfaces in solution. *Journal of chemical theory and computation* **2019**, *16*, 528–552.

(43) Ivani, I.; Dans, P. D.; Noy, A.; Pérez, A.; Faustino, I.; Hospital, A.; Walther, J.;

Andrio, P.; Goñi, R.; Balaceanu, A.; others Parmbsc1: a refined force field for DNA simulations. *Nature methods* **2016**, *13*, 55–58.

(44) Izadi, S.; Anandakrishnan, R.; Onufriev, A. V. Building water models: a different approach. *The Journal of Physical Chemistry Letters* **2014**, *5*, 3863–3871.

(45) Hopkins, C. W.; Le Grand, S.; Walker, R. C.; Roitberg, A. E. Long-time-step molecular dynamics through hydrogen mass repartitioning. *Journal of Chemical Theory and Computation* **2015**, *11*, 1864–1874.

(46) Ryckaert, J.-P.; Ciccotti, G.; Berendsen, H. J. Numerical integration of the cartesian equations of motion of a system with constraints: molecular dynamics of n-alkanes. *Journal of Computational Physics* **1977**, *23*, 327–341.

(47) Humphrey, W.; Dalke, A.; Schulten, K. VMD: visual molecular dynamics. *Journal of Molecular Graphics* **1996**, *14*, 33–38.

(48) DeLano, W. L.; others Pymol: An open-source molecular graphics tool. *CCP4 Newsl. Protein Crystallogr* **2002**, *40*, 82–92.

(49) Roe, D. R.; Cheatham III, T. E. PTRAJ and CPPTRAJ: software for processing and analysis of molecular dynamics trajectory data. *Journal of Chemical Theory and Computation* **2013**, *9*, 3084–3095.

(50) Li, W.; Wang, W.; Takada, S. Energy landscape views for interplays among folding, binding, and allostery of calmodulin domains. *Proceedings of the National Academy of Sciences* **2014**, *111*, 10550–10555.

(51) Freeman, G. S.; Hinckley, D. M.; Lequieu, J. P.; Whitmer, J. K.; De Pablo, J. J. Coarse-grained modeling of DNA curvature. *The Journal of chemical physics* **2014**, *141*.

(52) Niina, T.; Brandani, G. B.; Tan, C.; Takada, S. Sequence-dependent nucleosome sliding in rotation-coupled and uncoupled modes revealed by molecular simulations. *PLoS computational biology* **2017**, *13*, e1005880.

(53) Terakawa, T.; Takada, S. RESPAC: method to determine partial charges in coarse-grained protein model and its application to DNA-binding proteins. *Journal of Chemical Theory and Computation* **2014**, *10*, 711–721.

(54) Weeks, S. D.; Grasty, K. C.; Hernandez-Cuebas, L.; Loll, P. J. Crystal structures of Lys-63-linked tri-and di-ubiquitin reveal a highly extended chain architecture. *Proteins: Structure, Function, and Bioinformatics* **2009**, *77*, 753–759.

(55) Terakawa, T.; Takada, S. Multiscale ensemble modeling of intrinsically disordered proteins: p53 N-terminal domain. *Biophysical journal* **2011**, *101*, 1450–1458.

(56) Morrison, E. A.; Baweja, L.; Poirier, M. G.; Wereszczynski, J.; Musselman, C. A. Nucleosome composition regulates the histone H3 tail conformational ensemble and accessibility. *Nucleic acids research* **2021**, *49*, 4750–4767.

(57) Kenzaki, H.; Koga, N.; Hori, N.; Kanada, R.; Li, W.; Okazaki, K.-i.; Yao, X.-Q.; Takada, S. CafeMol: a coarse-grained biomolecular simulator for simulating proteins at work. *Journal of Chemical Theory and Computation* **2011**, *7*, 1979–1989.

(58) Fierz, B.; Kilic, S.; Hieb, A. R.; Luger, K.; Muir, T. W. Stability of nucleosomes containing homogenously ubiquitylated H2A and H2B prepared using semisynthesis. *Journal of the American Chemical Society* **2012**, *134*, 19548–19551.

(59) Schultze, S.; Grubmüller, H. Time-lagged independent component analysis of random walks and protein dynamics. *Journal of Chemical Theory and Computation* **2021**, *17*, 5766–5776.

(60) Scherer, M. K.; Trendelkamp-Schroer, B.; Paul, F.; Pérez-Hernández, G.; Hoffmann, M.; Plattner, N.; Wehmeyer, C.; Prinz, J.-H.; Noé, F. PyEMMA 2: A software package for estimation, validation, and analysis of Markov models. *Journal of chemical theory and computation* **2015**, *11*, 5525–5542.

(61) Likas, A.; Vlassis, N.; Verbeek, J. J. The global k-means clustering algorithm. *Pattern recognition* **2003**, *36*, 451–461.

(62) Michaud-Agrawal, N.; Denning, E. J.; Woolf, T. B.; Beckstein, O. MDAnalysis: a toolkit for the analysis of molecular dynamics simulations. *Journal of Computational Chemistry* **2011**, *32*, 2319–2327.

(63) Hunter, J. D. Matplotlib: A 2D graphics environment. *Computing in Science & Engineering* **2007**, *9*, 90–95.

(64) Miller III, B. R.; McGee Jr, T. D.; Swails, J. M.; Homeyer, N.; Gohlke, H.; Roitberg, A. E. MMPBSA. py: an efficient program for end-state free energy calculations. *Journal of Chemical Theory and Computation* **2012**, *8*, 3314–3321.

(65) Shirts, M. R.; Chodera, J. D. Statistically optimal analysis of samples from multiple equilibrium states. *The Journal of chemical physics* **2008**, *129*.

(66) Tekpinar, M.; Neron, B.; Delarue, M. Extracting dynamical correlations and identifying key residues for allosteric communication in proteins by correlationplus. *Journal of Chemical Information and Modeling* **2021**, *61*, 4832–4838.

(67) Landré, V.; Revi, B.; Mir, M. G.; Verma, C.; Hupp, T. R.; Gilbert, N.; Ball, K. L. Regulation of transcriptional activators by DNA-binding domain ubiquitination. *Cell Death & Differentiation* **2017**, *24*, 903–916.

(68) Mattiroli, F.; Penengo, L. Histone ubiquitination: an integrative signaling platform in genome stability. *Trends in Genetics* **2021**, *37*, 566–581.

(69) nisch, C.; Hake, S. B. Histone H2A variants in nucleosomes and chromatin: more or less stable? *Nucleic Acids Res* **2012**, *40*, 10719–10741.

(70) Bowerman, S.; Hickok, R. J.; Wereszczynski, J. Unique Dynamics in Asymmetric macroH2A–H2A Hybrid Nucleosomes Result in Increased Complex Stability. *The Journal of Physical Chemistry B* **2018**, *123*, 419–427.

(71) Chakravarthy, S.; Luger, K. The histone variant macro-H2A preferentially forms ̈hybrid nucleosomes: *J Biol Chem* **2006**, *281*, 25522–25531.

(72) Ullner, M.; Woodward, C. E.; Jönsson, B. A Debye–Hückel theory for electrostatic interactions in proteins. *The Journal of chemical physics* **1996**, *105*, 2056–2065.

(73) Pan, A. C.; Roux, B. Building Markov state models along pathways to determine free energies and rates of transitions. *The Journal of chemical physics* **2008**, *129*.

(74) Chodera, J. D.; Noé, F. Markov state models of biomolecular conformational dynamics. *Current opinion in structural biology* **2014**, *25*, 135–144.